BŞEÜ Fen Bilimleri Dergisi
9(1), 433-452, 2022

BSEU Journal of Science
https://doi.org/10.35193/bseufbd.1075723

e-ISSN: 2458-7575 (https://dergipark.org.tr/tr/pub/bseufbd)

Araştırma Makalesi - Research Article

Comparative Quantum Chemical Analysis of Midaflur, a Fluorinated Aminoimidazoline

Bir Florlu Aminoimidazolin Olan Midaflur'un Karşılaştırmalı Kuantum Kimyasal Analizi

Sümeyya Serin[1*]

Geliş / Received: 18/02/2022 ***Revize / Revised: 16/05/2022*** ***Kabul / Accepted: 20/06/2022***

ABSTRACT

Inspired by the striking achievements of fluorine-containing heterocyclic compounds in pharmaceutical chemistry, in this study quantum chemical calculations were carried out on the midaflur compound, which has skeletal-muscle relaxant and central nervous system (CNS) depressant properties. First of all, the total energy (ΔE_{Total}), enthalpy (ΔH), and Gibbs free energy (ΔG) values for both tautomeric structures of midaflur were calculated and it was determined which form was more stable and the rest of the study was continued on this structure. For the stable amino form, the HF method and B3LYP/B3PW91 DFT functionals with different basis sets were used in order to examine the geometric parameters. The results were found to be in good agreement with the experimental values given in the literature. Furthermore, FT-IR analysis, Mulliken population analysis, frontier molecular orbital (FMO) analysis, natural bond orbital (NBO) analysis, nonlinear optical (NLO) properties, and electrostatic surface properties were studied in detail. In another part of the study, the logPow (logarithm of the n-octanol/water partition coefficient) value, which is the numerical expression of the lipophilicity of a drug for entry into the CNS, was estimated for midaflur. For this purpose, the calculations were repeated for the water and n-octanol phases using the universal solvation model based on density (SMD) for all the methodologies used in this study, and the free energies of solvation were predicted. It was concluded that the predictive power of the computational methods increased in the order of HF < B3PW91 < B3LYP.

Keywords- Midaflur, DFT, Mulliken Charges, NBO

ÖZ

Flor içeren heterosiklik bileşiklerin farmasötik kimyadaki dikkat çekici başarılarından esinlenilen bu çalışmada, iskelet-kas gevşetici ve merkezi sinir sistemi (MSS) depresan özelliklerine sahip midaflur bileşiği üzerinde kuantum kimyasal hesaplamalar yapılmıştır.Öncelikle midaflur'un her iki tautomerik yapısı için toplam enerji (ΔE_{Total}), entalpi (ΔH) ve Gibbs serbest enerji (ΔG) değerleri hesaplanarak hangi formun daha kararlı olduğu belirlendi ve çalışmaya bu yapı üzerinden devam edildi.Kararlı amino formuna ait geometrik parametreleri incelemek için HF yöntemi ve B3LYP/B3PW91 DFT fonksiyonelleri farklı temel setlerle kullanılmıştır.Sonuçların literatürde verilen deneysel değerlerle uyum içinde olduğu belirlenmiştir.Ayrıca FT-IR analizi, Mulliken popülasyon analizi, sınır moleküler orbital (FMO) analizi, doğal bağ orbital (NBO) analizi, doğrusal olmayan optik (NLO) özellikler ve elektrostatik yüzey özellikleri detaylı olarak incelenmiştir.Çalışmanın başka bir bölümünde, bir ilacın MSS'ye giriş için lipofilitesinin sayısal ifadesi olan $logP_{ow}$ (n-oktanol/su partisyon katsayısının logaritması) değeri midaflur için tahmin edilmiştir.Bu amaçla, bu çalışmada kullanılan tüm metodolojiler için yoğunluğa dayalı evrensel solvasyon modeli (SMD) kullanılarak su ve n-oktanol fazları için

[1]*Corresponding author contact: sumeyya.alatas@inonu.edu.tr (https://orcid.org/0000-0002-4637-1734)
Scientific and Technological Research Center, Inonu University, Malatya, Türkiye

BŞEÜ Fen Bilimleri Dergisi
9(1), 433-452, 2022

BSEU Journal of Science
https://doi.org/10.35193/bseufbd.1075723

e-ISSN:2458-7575 (https://dergipark.org.tr/tr/pub/bseufbd)

hesaplamalar tekrarlanmış ve solvasyon serbest enerji değerleri tahmin edilmiştir. Hesaplamalı yöntemlerin tahmin gücünün HF < B3PW91 < B3LYP sırasına göre arttığı sonucuna varılmıştır.

Anahtar Kelimeler- Midaflur, DFT, Mulliken Yükleri, NBO

I. INTRODUCTION

Heterocyclic compounds represent a fairly large class of compounds that play a crucial role in pure and applied chemistry. It is frequently encountered that heterocycles are used in many areas of biological and industrial importance [1]. Fluorinated heterocyclic compounds, which are the subgroup of heterocyclic compounds and are at the intersection of organic, heterocyclic, and fluoroorganic chemistry, take part among the products of technical importance. There are many studies in which remarkable changes in physicochemical and pharmacological properties are observed with the addition of at least one fluorine atom or fluorinated functional groups to an organic molecule [2,6]. With the addition of fluorine, changes in the properties of the molecule such as electronegativity, hardness, polarizability, and lipophilicity may motive this situation. Nowadays, approximately 20% of marketed drugs are fluoropharmaceuticals. Fludrocortisone, a synthetic corticosteroid with antiinflammatory and antiallergic properties, was the first fluoropharmaceutical. Inspired by the high activity of fluorinated corticosteroids, interest in the synthesis of fluorinated drug candidates has increased steadily over the past 60 years [7-9]. It is known that current fluorinated drugs mostly contain fluorine and trifluoromethyl groups in their structures. Midaflur (4-amino-2,2,5,5-tetrakis(trifluoromethyl)-3-imidazoline) is one of the synthetics flourinated aminoimidazolines that is highly substituted with trifluoromethyl groups. It was reported that the compound synthesized and its structure was elucidated by Middleton and Krespan in 1970, has apparent pharmacological activity as a muscle relaxant and central nervous system depressant as a result of clinical studies [10]. There are several studies about crystal structure analysis, pharmacological and toxicological effects of midaflur [11-14].

Nowadays, quantum chemistry is an emerging field and goes on to make considerable improvements, both in terms of computational methods that make maximum use of existing computer hardware and theoretical methods that provide increasingly accurate and effective approaches. Quantum chemical computations have taken an active part in the chemical sciences to provide theoretical estimations and meaningful interpretations of many features of experimental interest. [15-21]. From this point of view, in this work, it is aimed to perform structural analysis, Mulliken population analysis, frontier molecular orbital (FMO) analysis, solvation free energy predictions, natural bond orbital (NBO) analysis, nonlinear optical (NLO) analysis and electrostatic surface properties (ESP) for midaflur based on quantum chemical calculations.

II. COMPUTATIONAL METHOD

Whole theoretical calculations were carried out by using GAUSSIAN 09W package program [22]. The geometry optimization of midaflur has been performed by using Density Functional Theory functionals both B3LYP and B3PW91 with five different basis sets [23-26]. Also, calculations were repeated by using Hartree-Fock (HF) method with the same basis sets [27]. Analysis of the IR spectrum of midaflur was done by means of the VEDA 4XX program with regard to the percent potential energy distribution (PED %) analysis [28]. In the optimized structures of the midaflur, no imaginary frequency has been observed and that has verified the real minimum on the potential energy surface. GAUSSVIEW 5 molecular visualization program was utilized to visualize HOMO-LUMO diagrams and ESP maps [29]. Gauss-Sum 3.0 program was used to obtain the density of states (DOS) plots [30]. Considering the solvents, water and n-octanol phases were simulated using the SMD solvent model, a universal solvation model developed by Truhlar and coworkers [31]. It was developed specifically to predict solvation free energies.

III. RESULTS AND DISCUSSION

A. Molecular Geometry and Stability

The chemical structure of midaflur (1), which is an aminoimidazoline derivative, and another tautomeric structure (2) where the double bond can be located in the exocyclic position are shown in Figure 1. From the 1H NMR analysis of 15N-labeled midaflur, it was concluded that the compound exists as an amino tautomer rather than an imino tautomer [10,11]. For each tautomer, total energy (ΔE_{Total}), enthalpy (ΔH), and Gibbs free energy (ΔG) values were calculated by using B3LYP/6-31+G (d,p) level of theory. According to Figure 1, amino form 1 has the lowest ΔE_{Total}, ΔH and ΔG value. This result supports that the most stable structure is amino form 1. This

structure was regarded for other calculations in the study. The optimized structure and atomic labeling of midaflur is shown in Figure 2.

1

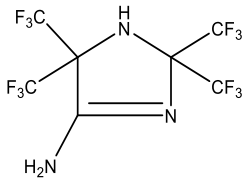

ΔE$_{Total}$=-1631.004186 a. u.

ΔH=-1630.855813 a. u.

ΔG=-1630.925476 a. u.

2

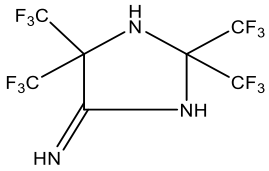

ΔE$_{Total}$=-1630.992408 a. u.

ΔH=-1630.844016 a. u.

ΔG=-1630.913856 a. u.

Figure 1. The chemical structures and physicochemical parameters of 1 and 2 calculated at B3LYP/6-31+G (d, p) level

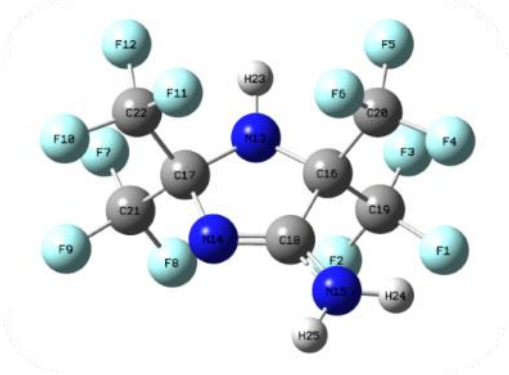

Figure 2. The optimized molecular structure of midaflur

The bond length and bond angle values of midaflur have been calculated by using DFT/B3LYP, DFT/B3PW91 with five basis sets, and HF method with four basis sets. For each methodology, calculated results have been compared with experimental values. The selected results are listed in Table 1,Tables S1 and S2. When the tables are examined, it is obvious that the values are compatible with each other. There are 12 C-F bonds in the structure of the title compound with bond lengths varying between 1.301 Å and 1.340 Å. The experimental and calculated C-F bond lengths are consistent for each methodology. Four C-N bond lengths with experimental values varying between 1.285 Å and 1.448 Å were calculated for B3LYP, B3PW91 and HF methods in the range of 1.281-1.467 Å, 1.280-1.460 Å and 1.259-1.451 Å, respectively. On the other hand, in accordance with the literature [32], it was seen that C-CF3 bond lengths were calculated in the range of 1.552-1.569 Å for B3LYP, 1.550-1.565 Å for B3PW91, and 1.542-1.550 Å for HF method. Considering the bond angles, mainly 12 F-C-F and 12 C-C-F bond angles were calculated. F-C-F bond angle values calculated for all methods ranged from 107.0 ˚ to 108.7˚, while C-C-F bond angle values ranged from 109.8˚ to 113.1˚. N15-C18-N14 bond angle with an experimental value of 124.8˚ was calculated in the range of 124.8-125.1˚, 124.7-125.0˚, and 124.9-125.1˚ for the B3LYP, B3PW91 and HF methods, respectively, and values very close to the X-ray value were obtained. In the calculations of bond length made with DFT/B3LYP, DFT/B3PW91 and HF methods with all basis sets, the linear correlation coefficients (R^2) were found to be around 0.99. Similarly, R^2 values were found to be around 0.97 in bond angle comparisons. All bond length and bond angle values are included in the calculation of R^2 values.

Table 1. Selected bond length and bond angle values calculated at B3LYP/6-311++G(d,p)

Bond length (Å)	X-ray data	6-311++G(d,p)	Bond Angle (°)	X-ray data	6-311++G(d,p)
N15-C18	1.315	1.346	N15-C18-N14	124.8	125.0
C18-N14	1.285	1.281	N13-C16-C19	110.7	110.3
N14-C17	1.432	1.435	N13-C16-C20	111.0	112.2
C17-N13	1.448	1.463	C17-C22-F10	112.8	113.1
N13-C16	1.431	1.439	C17-C21-F9	112.1	112.4
C16-C18	1.528	1.546	C16-C20-F6	110.9	110.9
C16-C19	1.539	1.565	C16-C19-F1	112.2	111.7
C17-C21	1.529	1.569	F10-C22-F11	107.5	107.9
C22-F10	1.301	1.335	F7-C21-F8	106.1	107.7
C21-F7	1.340	1.349	F6-C20-F5	107.3	107.5
C20-F6	1.334	1.338	F1-C19-F2	108.3	107.1
C19-F1	1.323	1.357	F2-C19-F3	107.2	108.3
	R^2	0.9896		R^2	0.9663

B. Vibrational Analysis

The vibrational analysis of midaflur was interpreted based on B3LYP/6-311++G (d, p) level of theory. The calculated FT-IR spectrum is represented in Figure 3. Analysis of the FT-IR spectrum of midaflur was done by using the VEDA 4XX program. The vibrational analysis results are represented in Table S3. As it can be seen from Table S3, 69 normal vibration modes were calculated for the midaflur molecule according to the 3N-6 formula. The vibrational modes were multiplied by 0.983 for vibrations less than 1700 cm^{-1} and the larger ones were multiplied by 0.958 scale factors for B3LYP/6-311++G (d,p) level of theory [33]. In the previously published study, it was stated that C=N absorption band was observed at 1695 cm^{-1}, according to the experimental results of midaflur [5]. When the theoretically calculated FT-IR values are examined, C=N asymmetric stretching vibration is observed at mainly 1652 cm^{-1} region (PED 81%). This vibration has the largest IR intensity value of 513.1 km/mol. In addition, the C=N symmetric stretching vibration is calculated as 1605 cm^{-1} (PED 11%).

In general, C-F stretching vibrations are observed in the range of 1000-1400 cm^{-1} in fluorinated compounds [32], in this study C-F symmetric stretching vibrations are measured theoretically at 1092 cm^{-1} (PED 24%), 1099 cm^{-1} (PED 54%), 1124 cm^{-1} (PED 56%) and 1193 cm^{-1} (PED 26%). Similarly, C-F asymmetric stretching vibrations are measured at 942 cm^{-1} (PED 34%), 1101 cm^{-1} (PED 20%), 1139 cm^{-1} (PED 52%) and 1206 cm^{-1} (PED 40%).

It has been observed that there are three NH vibrations from the theoretical FT-IR spectrum. First of all is the asymmetric stretching vibration of the N15-H bond observed at 3562 cm^{-1} (PED 99%). The second one is the N13-H symmetric stretching vibration observed at 3465 cm^{-1} (PED 100%). Finally, N15-H symmetric stretching vibration is observed at 3444 cm^{-1} (PED 99%). Bands are quite weak and their IR intensity values are calculated as 88.4, 56.4, and 105.6 km/mol respectively. Furthermore, the H24-N15-H25 and H23-N13-C17 symmetric bending vibrations were calculated as 1605 cm^{-1} (PED 71%) and 1420 cm^{-1} (PED 69%), respectively.

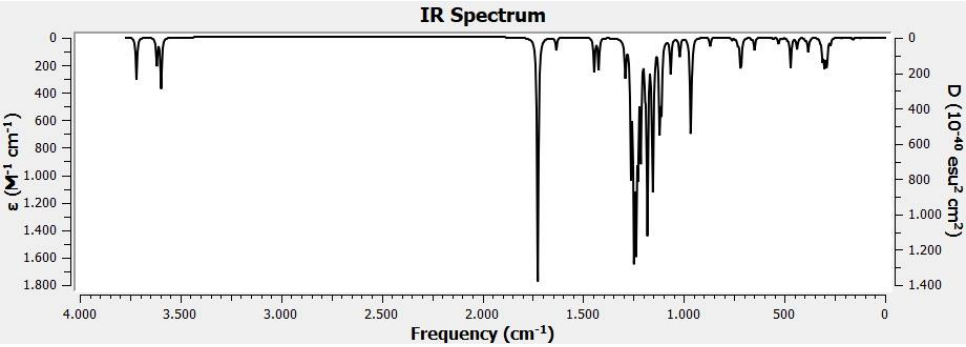

Figure 3. IR spectrum of midaflur at B3LYP/6-311++G(d,p) level of theory in gas phase

C. Mulliken Population Analysis

In this part of the study, Mulliken population analysis [34] was performed to determine charge changes for each atom of midaflur in gas and solvent environments. The calculations were carried out at B3LYP/6-311++G (d, p), B3PW91/6-311++G (d, p), and HF/6-311++G (d, p) levels of theory. The calculated results were listed in Table S4. It is clear from Figure 4, in which the atomic charge diagrams are presented, that there is a propensity in the same direction in the charge distribution at all three theory levels, including the solvent environment. For example, while for the H23 atom, at B3LYP/6-311++G (d, p) level, its charge in the gas phase was calculated as 0.37093e, an increase in the atomic charge was observed with the increase of the dielectric constant of the solvent environment. The charge of the H23 atom in n-octanol (ε=9.863) and water (ε=78.39) media was calculated as 0.42126e and 0.42977e, respectively. The same is true for other theory levels and H24 and H25 atoms. While the charges of negatively charged C16 and C17 atoms in the gas phase were -0.87062e and -4.05797e, respectively, these values increased to -0.85531e and -3.96336e in the n-octanol phase. In the water phase, it was calculated as -0.85169e and -3.94429e.

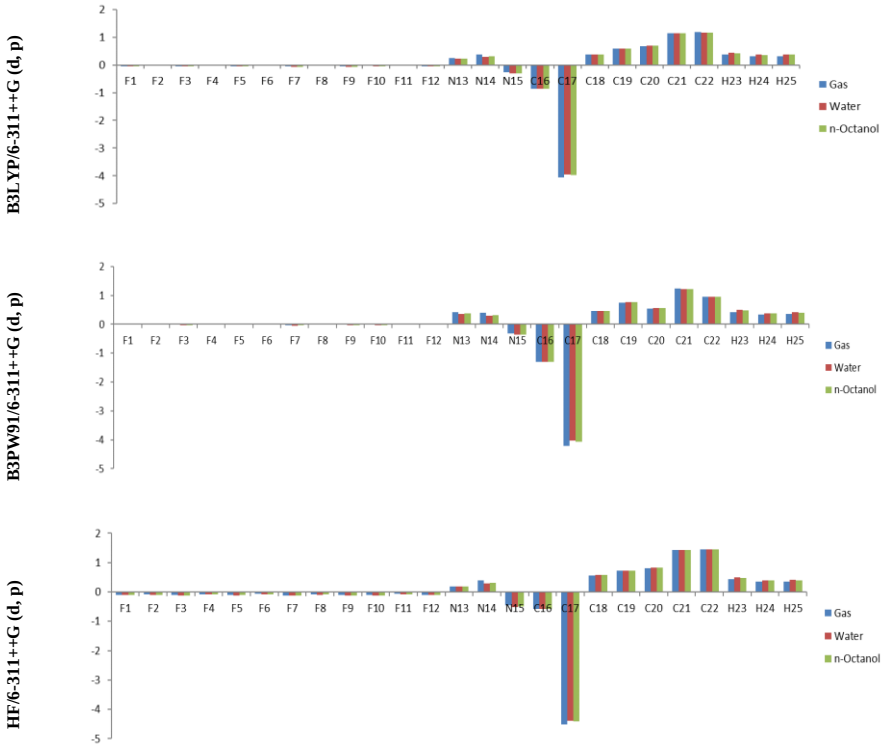

Figure 4. Mulliken charge diagrams of midaflur according to changing dielectric media

D. Frontier Molecular Orbital Analysis

DFT methods are convenient tools used not only to calculate molecular properties but also to obtain conceptual information about the chemical reactivity of molecules. The reactivity of a molecule can be interpreted with the assist of FMO theory [35]. The highest occupied molecular orbitals (HOMO) and the lowest unoccupied molecular orbitals (LUMO) refer to frontier molecular orbitals. LUMOs act as electron acceptors while HOMOs act as electron donors. The plots of DOS which describe energy levels and energy composition per unit energy increase can ensure an illustration of an entire orbitals system [36, 37]. The DOS graphs obtained from Gaussian outputs created at B3LYP/ 6-311++G(d,p) level for gas, water, and n-octanol phases using Gauss-Sum software are represented in Figure 5. Moreover, the HOMO-LUMO plots corresponding to the same phases are also shown in Figure 5. The green color of the molecular orbitals shown in DOS graphs represents the negative region while the red color corresponds to the positive region. The HOMO and LUMO locations of midaflur are largely distributed over the entire molecule, with the exception of some fluorine groups. The difference between HOMO and LUMO energies, known as the energy gap and symbolized by ΔE (Equation (3)), is clearly seen in the DOS graphs. It gives valuable information about the stability of a molecule.

BŞEÜ Fen Bilimleri Dergisi
9(1), 433-452, 2022

BSEU Journal of Science
https://doi.org/10.35193/bseufbd.1075723

e-ISSN:2458-7575 (https://dergipark.org.tr/tr/pub/bseufbd)

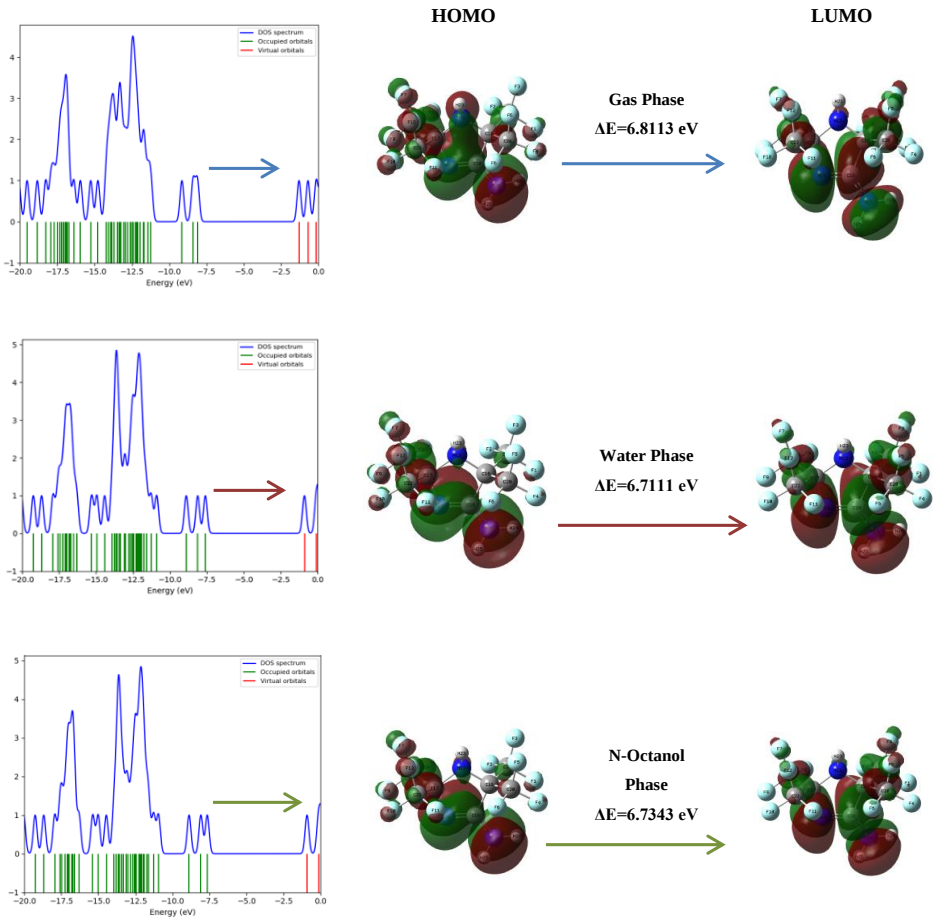

Figure 5. DOS diagrams and HOMO-LUMO plots of midaflur at B3LYP/6-311++G (d,p) level

As already known, in accordance with Koopmans theorem [38], the ionization energy (I) and electron affinity (A) (Equations 1 and 2) can be expressed via energies of HOMO and LUMO. Accordingly, if the HOMO and LUMO energy values are known, parameters called quantum chemical descriptors, which provide important information about the activity of the molecule, can be calculated. Quantum chemical descriptors, proposed by Parr et al. [39-43] and the corresponding formulas are given below (Equations 4-8) are frequently used by computational chemists.

Equation	Parameter	Equation Number
$I = -E_{HOMO}$	Ionization Potential (I)	(1)
$A = -E_{LUMO}$	Electron Affinity (A)	(2)
$\Delta E = E_{LUMO} - E_{HOMO}$	Energy Gap (ΔE)	(3)
$\mu = -\frac{I + A}{2}$	Chemical Potential (μ)	(4)
$\eta = \frac{I - A}{2}$	Chemical Hardness (η)	(5)
$S = \frac{1}{2\eta}$	Softness (S)	(6)
$\chi = \frac{I + A}{2}$	Electronegativity (χ)	(7)
$\omega = \frac{\mu^2}{2\eta}$	Electrophilicity index (ω)	(8)

E_{HOMO}, E_{LUMO}, ΔE values, and other quantum chemical descriptors calculated by using different methodologies in this study are represented in Table 2 for the gas, water and n-octanol phases. When the energy gap (Equation 3) values are examined, while generally similar values are obtained for B3LYP and B3PW91

functionals, a sharp increase is observed in the values obtained by the HF method. The change of basis sets for the B3LYP and B3PW91 functionals did not significantly affect the ΔE values. However, in the HF method, it was observed that the energy gaps decreased with the addition of diffuse functions [44] to the basis sets. The highest energy gap values of the title molecule are obtained by using HF method and the values are equal to 14.9880 eV, 14.8939 eV and 14.8460 eV for gas, n-octanol, and water phases respectively. The same trend was observed in chemical hardness values. Looking at Equations (3) and (5), it is easily understood that the energy gap and chemical hardness values are related to each other, so a trend in this direction is expected. Similarly, the highest chemical hardness values were also calculated as 7.4940 eV for gas phase, 7.4470 eV for n-octanol phase and 7.4230 eV for water phase using HF method.

One of the important quantum chemical descriptors is the electrophilicity index (ω), which is a measure of electrophilic strength. It is observed there is a similar trend in the EI values for not only B3LYP but also B3PW91 functionals. Additionally, the gradually increasing values according to the variation in the basis set draw attention. In the HF method, the electrophilicity index values for gas, n-octanol and water phases vary between 0.6864 eV and 0.9543 eV in the calculations made with the 6-31G (d, p) and 6-311G (d, p) basis sets. It is observed that these values increase with the addition of diffuse functions and change between 1.8060 eV and 2.2553 eV. The same situation can be seen for electronegativity values.

Table 2. Calculated quantum chemical descriptors for midaflur

				gas					
	Basis Set	E_{HOMO}	E_{LUMO}	ΔE	η (eV)	S (eV^{-1})	μ (eV)	χ) (eV)	ω (eV)
B3LYP	6-31G(d,p)	-7.4516	-0.5369	6.9147	3.4574	0.1446	-3.9943	3.9943	2.3073
	6-311G(d,p)	-7.8127	-0.8661	6.9466	3.4733	0.1440	-4.3394	4.3394	2.7107
	6-31++G(d,p)	-8.0271	-1.2553	6.7718	3.3859	0.1477	-4.6412	4.6412	3.1809
	6-311++G(d,p)	-8.1085	-1.2972	6.8113	3.4057	0.1468	-4.7029	4.7029	3.2471
B3PW91	6-31G(d,p)	-7.4815	-0.5676	6.9139	3.4570	0.1446	-4.0246	4.0246	2.3427
	6-311G(d,p)	-7.8121	-0.8604	6.9517	3.4759	0.1438	-4.3363	4.3363	2.7048
	6-31++G(d,p)	-7.9757	-1.1766	6.7991	3.3996	0.1471	-4.5762	4.5762	3.0800
	6-311++G(d,p)	-8.0540	-1.2193	6.8347	3.4174	0.1463	-4.6367	4.6367	3.1455
HF	6-31G(d,p)	-11.0511	3.9369	14.9880	7.4940	0.0667	-3.5571	3.5571	0.8442
	6-311G(d,p)	-11.2688	3.7078	14.9766	7.4883	0.0668	-3.7805	3.7805	0.9543
	6-31++G(d,p)	-11.3240	0.8923	12.2163	6.1082	0.0819	-5.2159	5.2159	2.2270
	6-311++G(d,p)	-11.4010	0.8768	12.2778	6.1389	0.0814	-5.2621	5.2621	2.2553
				water					
B3LYP	6-31G(d,p)	-7.0951	-0.2389	6.8562	3.4281	0.1459	-3.6670	3.6670	1.9613
	6-311G(d,p)	-7.3773	-0.5102	6.8671	3.4336	0.1456	-3.9438	3.9438	2.2649
	6-31++G(d,p)	-7.5354	-0.8637	6.6717	3.3359	0.1499	-4.1996	4.1996	2.6434
	6-311++G(d,p)	-7.6012	-0.8901	6.7111	3.3556	0.1490	-4.2457	4.2457	2.6859
B3PW91	6-31G(d,p)	-7.1604	-0.2920	6.8684	3.4342	0.1456	-3.7262	3.7262	2.0215
	6-311G(d,p)	-7.4173	-0.5298	6.8875	3.4438	0.1452	-3.9736	3.9736	2.2924
	6-31++G(d,p)	-7.5348	-0.8183	6.7165	3.3583	0.1489	-4.1766	4.1766	2.5971
	6-311++G(d,p)	-7.5966	-0.8419	6.7547	3.3774	0.1480	-4.2193	4.2193	2.6355
HF	6-31G(d,p)	-10.6111	4.2281	14.8392	7.4196	0.0674	-3.1915	3.1915	0.6864
	6-311G(d,p)	-10.7537	4.0923	14.8460	7.4230	0.0674	-3.3307	3.3307	0.7472
	6-31++G(d,p)	-10.8165	1.4161	12.2326	6.1163	0.0817	-4.7002	4.7002	1.8060
	6-311++G(d,p)	-10.8557	1.3998	12.2555	6.1278	0.0816	-4.7280	4.7280	1.8240

Table 2. Continues

		n-octanol							
B3LYP	6-31G(d,p)	-7.1125	-0.2370	6.8755	3.4378	0.1454	-3.6748	3.6748	1.9640
	6-311G(d,p)	-7.4132	-0.5274	6.8858	3.4429	0.1452	-3.9703	3.9703	2.2892
	6-31++G(d,p)	-7.5765	-0.8825	6.6940	3.3470	0.1494	-4.2295	4.2295	2.6723
	6-311++G(d,p)	-7.6442	-0.9099	6.7343	3.3672	0.1485	-4.2771	4.2771	2.7164
B3PW91	6-31G(d,p)	-7.1816	-0.2999	6.8817	3.4409	0.1453	-3.7408	3.7408	2.0334
	6-311G(d,p)	-7.4467	-0.5415	6.9052	3.4526	0.1448	-3.9941	3.9941	2.3103
	6-31++G(d,p)	-7.5694	-0.8327	6.7367	3.3684	0.1484	-4.2011	4.2011	2.6198
	6-311++G(d,p)	-7.6333	-0.8580	6.7753	3.3877	0.1476	-4.2457	4.2457	2.6605
HF	6-31G(d,p)	-10.6503	4.2311	14.8814	7.4407	0.0672	-3.2096	3.2096	0.6922
	6-311G(d,p)	-10.8027	4.0912	14.8939	7.4470	0.0671	-3.3558	3.3558	0.7561
	6-31++G(d,p)	-10.8620	1.3630	12.2250	6.1125	0.0818	-4.7495	4.7495	1.8452
	6-311++G(d,p)	-10.9063	1.3478	12.2541	6.1271	0.0816	-4.7793	4.7793	1.8640

E. Solvation Free Energy Calculations

Free energy of solvation, which is descriptive of the free energy of transfer of a particular molecule from the gas phase to solvent phase, has taken its place in recent studies as a topic of interest in computational chemistry [45-50]. Solvation free energy is a parameter needed in many fields such as chemistry, biology, and pharmacology, as it is closely related to some physicochemical properties such as solubility, interphase distribution, pKa, lipophilicity, and hydrophilicity. Unfortunately, out of millions of known organic molecules, those with known experimental solvation free energy values are in the minority. This situation allows scientists to turn toward computational methods provided that trustworthy predictions are obtained. In order to acquire information about the relative solubility of a solute in different dielectric media, solvation-free energies can be computed for the same solute with different solvents. Especially in drug design studies in pharmacology, the solvation free energy values obtained by using computational methods can be interpreted and information about the lipophilic character of a molecule can be obtained. The extent of the absorption, distribution, metabolism, and excretion (ADME) process of a drug largely depends on the structural and physicochemical properties of the drug. One of the leading of these physicochemical properties is lipophilicity [51-53]. The quantitative expression of the lipophilicity is thelogarithm of the partition coefficient (logP) that isacquired by measuring the partitioning of a solute between two immiscible solvents systems. The water/n-octanol solvent system is the most commonly used [54].

In the light of this information, in this part of the work, Gibbs free solvation energies of midaflur were computed for the water and n-octanol phases utilizing SMD solvent model at the studied theory levels. By using calculated solvation free energy values, one can calculate the partition coefficient, according to the expression given below [55] (Equation 9):

$$LogP_{ow} = \frac{(\Delta G_{water} - \Delta G_{n-octanol})}{2.303RT} \quad (9)$$

According to the formula, R and T express the gas constant and temperature, respectively. ΔGwater and ΔGn-octanol are the free energy differences of midaflur in solvent and in gas phase. The computed results are shown in Table 3 and logPow values were estimated for each level. The experimental n-octanol/water partition coefficient of midaflur ($logP_{ow}$= 3.35) was taken from reference [56]. In accordance with Table 3, it is marked that the solvation free energy values decrease when going from the water phase into the n-octanol phase. Moreover, it is observed that calculations with basis sets including diffuse functions tend to produce lower solvation free energies not only in water but also in n-octanol phases. The closest result to the logPow value given in the literature was obtained by B3LYP/6-31G (d, p) level of theory with 1.41 logarithmic unit deviation. It can be said that the predictive power of the computational methods increases in the following order: HF < B3PW91 < B3LYP.

Table 3. The Calculated solvation free energy and $logP_{ow}$ values of midaflur

Method	ΔG_{solv} (kcal/mol)		
B3LYP	ΔG_w	ΔG_{oct}	**$LogP_{ow}$ (calc.)**
6-31G (d, p)	-5.45	-8.10	1.94
6-311G (d, p)	-6.59	-8.33	1.28
6-31++G (d, p)	-7.11	-8.42	0.96
6-311++G (d, p)	-7.45	-8.81	0.99
B3PW91			
6-31G (d, p)	-5.49	-6.92	1.05
6-311G (d, p)	-6.54	-8.20	1.21
6-31++G (d, p)	-6.86	-8.29	1.04
6-311++G (d, p)	-7.08	-8.60	1.11
HF			
6-31G (d, p)	-7.01	-8.22	0.89
6-311G (d, p)	-7.91	-8.93	0.75
6-31++G (d, p)	-7.85	-9.09	0.91
6-311++G (d, p)	-8.33	-9.35	0.75

F. Natural Bond Orbital (NBO) Analysis

In computational chemistry, NBO analysis is a popular tool that is frequently used to examine intermolecular and intramolecular bond interactions. It is realized by taking into account all possible interactions between the donor (i) Lewis type NBOs and the acceptor (j) non-Lewis type NBOs and by predicting its energy values with the second order perturbation theory. For each donor (i) and acceptor (j) NBO, the stabilization energy $E^{(2)}$ value is calculated according to the formula as follows (Equation 10):

$$E^{(2)} = \Delta E_{ij} = qi\frac{(Fij)^2}{(\varepsilon j - \varepsilon i)} \quad (10)$$

In the formula, qi, εj, and εi, Fij represent donor bonding orbital occupancy, acceptor bond orbital energies and NBO Fock matrix element respectively [57, 58]. The stabilization energy $E^{(2)}$ expresses the intensity of electron delocalization between the bonding (BD) or lone pair (LP) orbitals and anti-bonding (BD*) orbitals. The higher $E^{(2)}$ value means that the interaction between the donor and acceptor orbitals is more intensive.

In this study, the NBO analysis of midaflur has been calculated by using B3LYP/6-311++G (d, p) level of theory in gas phase. The calculated natural population analysis (NPA) and natural electronic configuration (NEC) results for each atom are summarized in Table 4. According to NBO analysis, the Lewis natural bond orbitals describe 98.6% of the total electron density and the remaining non-Lewis density found valence shell antibonds is about 1.12%, Rydberg antibonds about 0.24% of total electron density. The second-order perturbation theory results of Fock matrix in NBO basis for midaflur are shown in Table 5. There are three **L**one **P**air interactions LP (1), LP (2), and LP (3) of each fluorine atom. Among them, the strongest interactions have been observed between LP (3) of each fluorine atom and neighboring fluorine and carbon atoms. Stabilization energies vary between 8.37 and 12.68 kcal/mol. In addition, the 13 interactions of lone pair LP (1) of N13, 8 interactions of LP (1) of N14, and 4 interactions of LP (1) of N15 have been determined from NBO analysis results. For N13, four interactions are significant. The stabilization energies for the interactions LP (1) N13→ σ*(C16-C19), N13→ σ*(C16-C20), N13→ σ*(C17-C21), N13→ σ*(C17-C22) are calculated as 8.65, 6.26, 7.33, and 5.14 kcal/molrespectively. For N14, there are three important interactions which are LP (1) N14→ σ*(N13-C17), N14→ σ*(N15-C18), and N14→ σ*(C16-C18). The stabilization energies are 6.07, 2.54, and 12.26 kcal/mol respectively. Finally, the strongest electron delocalization is observed between LP (1) N15 donor and π*(N14-C18) acceptor orbitals, the stabilization energy is calculated as 58.63 kcal/mol.

Table 4. Results of NPA and NEC of Midaflur

Natural Population						
Atom	**Natural Charge**	**Core**	**Valence**	**Rydberg**	**Total**	**Natural Electron Configuration**
F1	-0.36221	1.99992	7.35454	0.00775	9.36221	[core]$2S^{1.85}2p^{5.50}$
F2	-0.33153	1.99991	7.32324	0.00838	9.33153	[core]$2S^{1.84}2p^{5.48}$
F3	-0.34094	1.99991	7.33303	0.00800	9.34094	[core]$2S^{1.85}2p^{5.49}$
F4	-0.34663	1.99991	7.33893	0.00779	9.34663	[core]$2S^{1.85}2p^{5.49}$
F5	-0.34761	1.99991	7.33986	0.00783	9.34761	[core]$2S^{1.85}2p^{5.49}$
F6	-0.33540	1.99991	7.32700	0.00848	9.33540	[core]$2S^{1.85}2p^{5.48}$
F7	-0.35327	1.99991	7.34550	0.00785	9.35327	[core]$2S^{1.85}2p^{5.50}$
F8	-0.34327	1.99991	7.33463	0.00873	9.34327	[core]$2S^{1.85}2p^{5.49}$
F9	-0.33972	1.99991	7.33215	0.00766	9.33972	[core]$2S^{1.85}2p^{5.49}$
F10	-0.33422	1.99991	7.32663	0.00768	9.33422	[core]$2S^{1.84}2p^{5.48}$
F11	-0.34309	1.99991	7.33433	0.00885	9.34309	[core]$2S^{1.85}2p^{5.49}$
F12	-0.35881	1.99992	7.35126	0.00763	9.35881	[core]$2S^{1.85}2p^{5.50}$
N13	-0.68684	1.99936	5.66592	0.02156	7.68684	[core]$2S^{1.28}2p^{4.39}3p^{0.01}$
N14	-0.52912	1.99924	5.50679	0.02308	7.52912	[core]$2S^{1.38}2p^{4.13}3p^{0.01}3d^{0.01}$
N15	-0.75795	1.99935	5.74430	0.01430	7.75795	[core]$2S^{1.30}2p^{4.45}3p^{0.01}$
C16	-0.06018	1.99891	4.03033	0.03094	6.06018	[core]$2S^{0.97}2p^{3.07}3d^{0.01}4p^{0.02}$
C17	0.16866	1.99906	3.79377	0.03851	5.83134	[core]$2S^{0.93}2p^{2.86}3d^{0.01}4p^{0.02}$
C18	0.46833	1.99909	3.49320	0.03938	5.53167	[core]$2S^{0.78}2p^{2.71}3d^{0.01}4p^{0.02}$
C19	1.07637	1.99923	2.85846	0.06594	4.92363	[core]$2S^{0.78}2p^{2.08}4S^{0.01}3d^{0.02}4p^{0.03}$
C20	1.07378	1.99922	2.86174	0.06526	4.92622	[core]$2S^{0.78}2p^{2.08}4S^{0.01}3d^{0.02}4p^{0.03}$
C21	1.07276	1.99921	2.86204	0.06600	4.92724	[core]$2S^{0.78}2p^{2.08}4S^{0.01}3d^{0.02}4p^{0.03}$
C22	1.06849	1.99920	2.86725	0.06505	4.93151	[core]$2S^{0.79}2p^{2.08}4S^{0.01}3d^{0.02}4p^{0.03}$

Table 5. Second-order perturbation theory analysis of Midaflur at B3LYP/6-311++G (d,p) level of theory in gas phase

Donor(i)	**Occupancy**	**Acceptor(j)**	**Occupancy**	**$E^{(2)}$ kcal/mol**	**E(j)-E(i)/a.u**	**F(i,j)/a.u**
πN14-C18	1.93788	σ*C17-C21	0.10048	5.19	0.61	0.051
		σ*C17-C22	0.09496	5.69	0.60	0.053
σC16-C19	1.97675	π*N14-C18	0.27940	1.64	0.70	0.032
σC16-C20	1.97761	π*N14-C18	0.27940	1.74	0.70	0.033
σC17-C21	1.97622	σ*F11-C22	0.08685	1.46	0.90	0.033
σC17-C22	1.97822	σ*F8-C21	0.08632	1.36	0.92	0.032
LP (2) F1	1.95307	σ*C16-C19	0.09412	6.27	0.70	0.060
LP (3) F1	1.94152	σ*F2-C19	0.08370	8.37	0.68	0.068
		σ*F3-C19	0.08904	11.17	0.67	00.78
LP (2) F2	1.94515	σ*C16-C19	0.09412	7.15	0.70	0.064
LP (3) F2	1.93326	σ*F1-C19	0.09740	11.85	0.64	0.078
		σ*F3-C19	0.08904	10.54	0.66	0.075
LP (2) F3	1.94902	σ*C16-C19	0.09412	6.63	0.70	0.061
LP (3) F3	1.93455	σ*F1-C19	0.09740	12.60	0.64	0.081
		σ*F2-C19	0.08370	8.94	0.67	0.069
LP (2) F4	1.95018	σ*C16-C20	0.08584	6.90	0.70	0.063
LP (3) F4	1.93660	σ*F5-C20	0.09281	11.91	0.66	0.080
		σ*F6-C20	0.08653	9.06	0.67	0.070
LP (2) F5	1.95065	σ*C16-C20	0.08584	6.22	0.70	0.060
LP (3) F5	1.93729	σ*F4-C20	0.09275	11.54	0.66	0.078
		σ*F6-C20	0.08653	9.18	0.67	0.070
LP (2) F6	1.94675	σ*C16-C20	0.08584	6.98	0.70	0.063
LP (3) F6	1.93415	σ*F4-C20	0.09275	11.71	0.65	0.079
		σ*F5-C20	0.09281	10.20	0.65	0.073
LP (2) F7	1.95174	σ*C17-C21	0.10048	6.37	0.69	0.060
LP (3) F7	1.93874	σ*F8-C21	0.08632	10.20	0.67	0.074
		σ*F9-C21	0.08664	10.38	0.67	0.075
LP (2) F8	1.94703	σ*C17-C21	0.10048	6.70	0.69	0.062
LP (3) F8	1.93775	σ*F7-C21	0.09200	11.91	0.65	0.079
		σ*F9-C21	0.08664	9.52	0.67	0.072
LP (2) F9	1.94832	σ*C17-C21	0.10048	7.21	0.69	0.064
LP (3) F9	1.93544	σ*F7-C21	0.09200	11.71	0.65	0.079
		σ*F8-C21	0.08632	9.96	0.66	0.073

Table 5. Continues

LP (2) F10	1.94720	σ*C17-C22	0.09496	7.25	0.70	0.064
LP (3) F10	1.93306	σ*F11-C22	0.08685	9.51	0.66	0.071
		σ*F12-C22	0.09470	12.68	0.65	0.081
LP (2) F11	1.94787	σ*C17-C22	0.09496	6.62	0.70	0.061
LP (3) F11	1.93662	σ*F10-C22	0.08569	10.71	0.67	0.076
		σ*F12-C22	0.09470	10.76	0.65	0.075
LP (2) F12	1.95317	σ*C17-C22	0.09496	5.95	0.70	0.058
LP (3) F12	1.94060	σ*F10-C22	0.08569	10.10	0.67	0.074
		σ*F11-C22	0.08685	9.80	0.67	0.073
LP (1) N13	1.87877	σ*C16-C19	0.09412	8.65	0.55	0.062
		σ*C16-C20	0.08584	6.26	0.55	0.053
		σ*C17-C21	0.10048	7.33	0.56	0.058
		σ*C17-C22	0.09496	5.14	0.56	0.048
LP (1) N14	1.89714	σ*N13-C17	0.04313	6.07	0.68	0.058
		σ*N15-C18	0.02763	2.54	0.84	0.042
		σ*C16-C18	0.06436	12.26	0.69	0.083
LP (1) N15	1.73410	π*N14-C18	0.27940	58.63	0.29	0.117

G. NLO Analysis

The nonlinear optical properties of molecular materials are widely studied area, both experimentally and theoretically, as this would be a very promising advance for molecular electronics. It is known that in order to obtain highly active nonlinear optical materials, it is necessary to design microscopic entities with large hyperpolarizabilities [59-61]. In this study, in order to explore the NLO properties of midaflur, dipole moment (μi), polarizability (αij) and first-order hyperpolarizability (βijk) values were computed at B3LYP/6–311++G (d, p) level for gas, water and n-octanol environments. Here, each subscript of i, j, k, specifies the indices of the Cartesian axes x, y, z. Based on this information, using the data obtained from the Gaussian output files, the total dipole moment (μ_{tot}), mean polarizability (α_{tot}), anisotropic polarizability (Δα) and mean first hyperpolarizability (β_{tot}) values were calculated according to the formulas given below (Equations 11-14) [62, 63].

$$\mu_{tot} = \sqrt{(\mu_x^2 + \mu_y^2 + \mu_z^2)} \tag{11}$$

$$\alpha_{tot} = \frac{1}{3}(\alpha_{xx} + \alpha_{yy} + \alpha_{zz}) \tag{12}$$

$$\Delta\alpha = \frac{1}{\sqrt{2}}\left[(\alpha_{xx} - \alpha_{yy})^2 + (\alpha_{yy} - \alpha_{zz})^2 + (\alpha_{zz} - \alpha_{xx})^2 + 6\alpha_{xz}^2 + 6\alpha_{xy}^2 + 6\alpha_{yz}^2\right]^{\frac{1}{2}} \tag{13}$$

$$\beta_{tot} = \left[(\beta_{xxx} + \beta_{xyy} + \beta_{xzz})^2 + (\beta_{yyy} + \beta_{yzz} + \beta_{yxx})^2 + (\beta_{zzz} + \beta_{zxx} + \beta_{zyy})^2\right]^{\frac{1}{2}} \tag{14}$$

The data from the output files and the calculated values are listed in Table 6. The dependence of the dipole moment values on the solvent environment is clearly seen from Table 6. As the dielectric constant of the medium increased, the dipole moment also increased. Midaflur is highly polar in the x-direction compared to the other components (μ_x = 3.0726 D (gas), 4.4871 D (n-octanol), 4.7809 D (water)). The total dipole moment values calculated at the B3LYP/6-311++G (d, p) theory level were found to be 3.6962 D, 5.2474 D and 5.6182 D for the gas, water and n-octanol phases, respectively.

Since the polarizability (α_{ij}) and first-order hyperpolarizability (β_{ijk}) values presented in the Gaussian output files are given in atomic units (a. u.), the calculated values are converted to electrostatic units (esu) (α: 1 a. u. = 0.1482 x10^{-24} esu; β: 1 a. u. = 8.6393 x10^{-33} esu) for easier interpretation [64]. Accordingly, the mean polarizability values (α_{tot}) were calculated as -17.98x10^{-24} esu, -18.01x10^{-24} esu and -18.02x10^{-24} esu for gas, n-octanol and water phases, respectively. It was observed that the anisotropic polarizability values (Δα) increased

according to the polarity of the medium and were calculated as $3.24x10^{-24}$ esu (gas phase), $4.198x10^{-24}$ esu (n-octanol phase) and $4.274x10^{-24}$ esu (water phase). In addition, mean first-order hyperpolarizability values, which are significant parameters in determining the NLO property, were calculated as $321.6x10^{-33}$ esu for gas phase, $525.4x10^{-33}$ esu for n-octanol phase, and finally $562.7x10^{-33}$ esu for water phase. The effect of the solvent environment was also observed in these values. When the first hyperpolarizability value (β_{tot} = $372.8x10^{-33}$ esu) [65, 66] of the urea molecule, which is frequently used as a reference substance for the evaluation of the results in NLO property analysis studies, is compared with the calculation results of midaflur, it is seen that the water and n-octanol phase values are higher.

Table 6. Dipole moment, polarizability and first-order hyperpolarizability values according to changing dielectric media

	Dipole moment (D)				First Order Hyperpolarizability (a. u.)		
	gas	**n-octanol**	**water**		**gas**	**n-octanol**	**water**
μ_x	3.0726	4.4871	4.7809	β_{xxx}	11.8102	22.7796	25.1148
μ_y	0.2870	0.9668	1.2287	β_{xxy}	0.2120	1.6493	1.8607
μ_z	2.0344	2.5430	2.6828	β_{xyy}	-0.2239	0.7932	1.0586
μ_{tot}	3.6962	5.2474	5.6182	β_{yyy}	2.2386	2.5087	3.2367
	Polarizability (a. u.)			β_{xxz}	5.1097	8.4541	8.8101
α_{xx}	-126.4922	-128.0979	-128.0822	β_{xyz}	-2.9204	-0.6376	-0.722
α_{xy}	-1.3313	-0.4486	-0.5321	β_{yyz}	-8.4574	-8.5471	-8.8184
α_{yy}	-127.0261	-128.8750	-128.8279	β_{xzz}	21.8106	29.0096	30.1493
α_{xz}	7.8080	10.8542	11.3475	β_{yzz}	-2.5152	1.8543	2.3522
α_{yz}	-2.6069	-1.9316	-2.3525	β_{zzz}	19.8030	30.053	31.8557
α_{zz}	-110.3675	-107.5905	-107.7763	β_x	33.3969	52.5824	56.3227
α_{tot}	-121.2953	-121.5211	-121.5621	β_y	-0.0650	6.012	7.450
$\Delta\alpha$	21.8518	28.3255	28.8405	β_z	16.4553	29.96	31.8474
				β_{tot}	37.2310	60.817	65.131

H. Molecular Electrostatic Potential (MEP)

MEP surfaces are descriptive of the three-dimensional charge distributions within the molecule. The MEP surface diagram of a particular molecule is a significant diagram in terms of representation of positive, negative and neutral electrostatic potential regions depending on the color gradation [67-69]. It is a method often used by computational chemists in order to forecast the reactive locations of electrophilic and nucleophilic attacks in the studied molecule. In this study, the molecular electrostatic potential (MEP), electrostatic potential (ESP), total density and contour maps of midaflur at B3LYP/6-311++G (d, p) level are shown in Figure 6. The 3D maps of MEP, ESP and total density of title molecule are in the ranges -24.2 kcal/mol (red) and 24.2 kcal/mol (blue), −5.9 kcal/mol (red) and 5.9 kcal/mol (blue), -0.26 kcal/mol (red) and 0.26 kcal/mol (blue) respectively. The electrostatic potential decreases according to the order blue > green > yellow > orange > red. As seen in the MEP map in Figure 6, the blue zones are largely localized around NH and NH_2. Furthermore, the red- and orange-colored zones are concentrated around the fluorine groups attached to the C21 and C22 carbons. In this way, the most convenient sites for nucleophilic and electrophilic attacks are predicted.

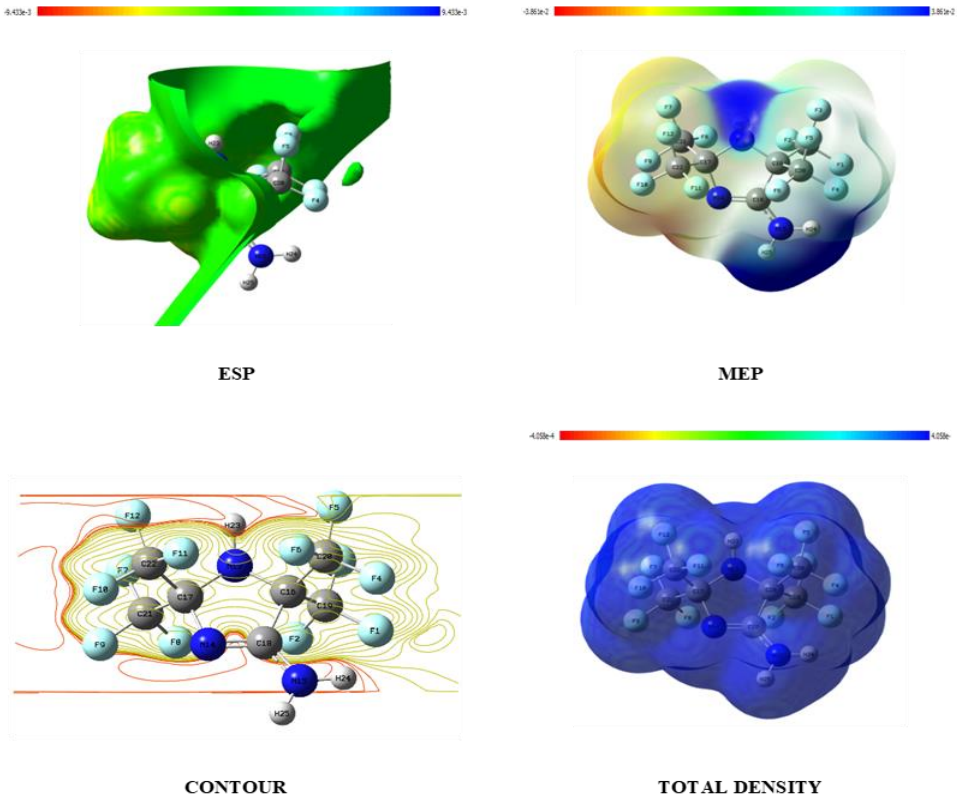

Figure 6. Molecular surfaces calculated at B3LYP/6-311++G (d, p) level of theory for water phase

VI. CONCLUSION

The discovery of highly active fluoropharmaceuticals has greatly accelerated the studies on the synthesis of new fluorinated heterocyclic compounds. It has been a source of inspiration for both experimental and theoretical studies. In this context, in this study, it was aimed to implement quantum chemical calculations in order to evaluate the structural, spectroscopic and electronic properties of midaflur, a perfluorinated N-heterocyclic compound, about which there are limited studies. In the first step, the determination of the stable tautomeric structure was performed by calculating the thermodynamic parameters ΔE, ΔH and ΔG using the B3LYP functional and the 6-31+G(d, p) basis set. The results acquired from these calculations confirmed the stable amino structure. further calculations were continued by using the B3LYP and B3PW91 DFT functionals and the HF method with the basis sets 6-31G(d, p), 6-311G (d, p), 6-31++G(d, p) and 6-311++G(d, p). Geometric parameters for midaflur were found to have significant correlations of 99% in terms of bond length and 96% in terms of bond angle with the values available in the literature. Analysis results of the FT-IR spectrum of studied molecule were presented in tabular form. Mulliken atomic charges of each atom of midaflur have been determined and the changes on going from gas phase to solvent phase have been noted. In addition, the variation of the calculated quantum chemical descriptors, which helps to explain the stability and bioactivity, depending on the method and solvent phase was investigated. For the energy range values, the addition of diffuse functions to the basis sets in B3LYP and B3PW91 functionals did not significantly affect the results, while the values decreased in the HF method.

The commonly used method for determining lipophilicity, which is an important physicochemical parameter in pharmacology, is the determination of the n-octanol/water partition coefficient expressed as logPow. In this study, $\log P_{ow}$ estimation was made using Gibbs solvation free energy for each methodology. The closest result to the literature value was obtained at the B3LYP/6-31G (d, p) theory level. It was concluded that the predictive power of the computational methods increased in the following order: HF < B3PW91 < B3LYP. NPA and NBO of midaflur were analyzed to get detailed information about charge distribution and intramolecular interactions. According to the calculated results that were tabulated in Table 4, the strongest electron delocalization was observed between LP (1) N15 donor and π*(N14-C18) acceptor orbitals, the stabilization energy was calculated as 58.63 $kcalmol^{-1}$. The striking point in the NLO properties calculated at the B3LYP/6-311++G (d,p)

theory level is the dependence of the dipole moment, polarizability and first order hyperpolarizability values on the solvent environment. Water and n-octanol phase values were found to be higher than the values of urea used as a reference substance in NLO studies. Finally, from results of electrostatic surface property analysis, the most convenient sites for nucleophilic and electrophilic attacks were predicted.

SUPPLEMENTARY MATERIALS

Table S1. Selected bond length values calculated at B3LYP, B3PW91, and HF

B3LYP						
Bond length (Å)	**X-ray data**	**6-31G(d,p)**	**6-311G(d,p)**	**6-31+G(d,p)**	**6-31++G(d,p)**	
N15-C18	1.315	1.350	1.346	1.348	1.348	
C18-N14	1.285	1.284	1.281	1.286	1.286	
N14-C17	1.432	1.439	1.436	1.436	1.436	
C17-N13	1.448	1.467	1.465	1.464	1.465	
N13-C16	1.431	1.442	1.439	1.440	1.440	
C16-C18	1.528	1.540	1.542	1.546	1.546	
C16-C19	1.539	1.554	1.559	1.565	1.565	
C17-C21	1.529	1.557	1.562	1.569	1.568	
C22-F10	1.301	1.337	1.335	1.340	1.340	
C21-F7	1.340	1.349	1.348	1.353	1.353	
C20-F6	1.334	1.340	1.337	1.342	1.342	
C19-F1	1.323	1.360	1.357	1.361	1.361	
	R^2	0.9913	0.9906	0.9903	0.9905	
B3PW91						
Bond length (Å)	**X-ray data**	**6-31G(d,p)**	**6-311G(d,p)**	**6-31+G(d,p)**	**6-31++G(d,p)**	**6-311++G(d,p)**
N15-C18	1.315	1.345	1.342	1.344	1.344	1.343
C18-N14	1.285	1.284	1.280	1.285	1.285	1.281
N14-C17	1.432	1.432	1.429	1.431	1.431	1.429
C17-N13	1.448	1.460	1.458	1.458	1.458	1.457
N13-C16	1.431	1.436	1.433	1.434	1.435	1.433
C16-C18	1.528	1.536	1.536	1.540	1.540	1.539
C16-C19	1.539	1.552	1.555	1.561	1.561	1.560
C17-C21	1.529	1.555	1.559	1.565	1.565	1.564
C22-F10	1.301	1.333	1.330	1.335	1.335	1.330
C21-F7	1.340	1.345	1.343	1.348	1.348	1.344
C20-F6	1.334	1.335	1.332	1.337	1.337	1.332
C19-F1	1.323	1.354	1.352	1.355	1.355	1.351
	R^2	0.9915	0.9904	0.9902	0.9904	0.9897
HF						
Bond length (Å)	**X-ray data**	**6-31G(d,p)**	**6-311G(d,p)**	**6-31++G(d,p)**	**6-311++G(d,p)**	
N15-C18	1.315	1.338	1.338	1.339	1.340	
C18-N14	1.285	1.262	1.259	1.263	1.259	
N14-C17	1.432	1.428	1.427	1.428	1.427	
C17-N13	1.448	1.451	1.450	1.450	1.450	
N13-C16	1.431	1.431	1.431	1.432	1.432	
C16-C18	1.528	1.533	1.534	1.536	1.537	
C16-C19	1.539	1.543	1.545	1.548	1.549	
C17-C21	1.529	1.544	1.546	1.549	1.550	
C22-F10	1.301	1.311	1.306	1.312	1.306	
C21-F7	1.340	1.321	1.317	1.322	1.317	
C20-F6	1.334	1.312	1.306	1.312	1.307	
C19-F1	1.323	1.326	1.321	1.326	1.321	
	R^2	0.9885	0.9862	0.9875	0.9851	

BŞEÜ Fen Bilimleri Dergisi
9(1), 433-452, 2022

BSEU Journal of Science
https://doi.org/10.35193/bseufbd.1075723

e-ISSN: 2458-7575 (https://dergipark.org.tr/tr/pub/bseufbd)

Table S2. Selected bond angle values calculated at B3LYP, B3PW91, and HF

B3LYP					
Bond Angle (°)	**X-ray data**	**6-31G(d,p)**	**6-311G(d,p)**	**6-31+G(d,p)**	**6-31++G(d,p)**
N15-C18-N14	124.8	125.1	125.1	124.8	124.8
N13-C16-C19	110.7	110.1	110.2	110.3	110.3
N13-C16-C20	111.0	112.0	112.1	112.2	112.2
C17-C22-F10	112.8	112.8	113.0	113.1	113.1
C17-C21-F9	112.1	112.1	112.3	112.5	112.5
C16-C20-F6	110.9	110.9	110.9	110.9	110.9
C16-C19-F1	112.2	111.5	111.7	111.8	111.8
F10-C22-F11	107.5	108.2	108.0	107.9	107.9
F7-C21-F8	106.1	108.1	107.8	107.8	107.8
F6-C20-F5	107.3	107.7	107.6	107.5	107.5
F1-C19-F2	108.3	107.2	107.1	107.0	107.0
	R^2	0.9486	0.9622	0.9674	0.9664

B3PW91						
Bond Angle (°)	**X-ray data**	**6-31G(d,p)**	**6-311G(d,p)**	**6-31+G(d,p)**	**6-31++G(d,p)**	**6-311++G(d,p)**
N15-C18-N14	124.8	125.0	125.0	124.8	124.7	124.9
N13-C16-C19	110.7	110.2	110.3	110.3	110.3	110.3
N13-C16-C20	111.0	112.1	112.2	112.3	112.2	112.2
C17-C22-F10	112.8	112.8	113.0	113.1	113.1	113.1
C17-C21-F9	112.1	112.1	112.2	112.4	112.4	112.4
C16-C20-F6	110.9	110.9	110.1	110.9	110.9	110.8
C16-C19-F1	112.2	111.6	111.7	111.8	111.8	111.8
F10-C22-F11	107.5	108.1	107.9	107.9	107.9	107.9
F7-C21-F8	106.1	108.1	107.9	107.8	107.8	107.7
F6-C20-F5	107.3	107.7	107.5	107.6	107.5	107.5
F1-C19-F2	108.3	107.2	107.1	107.0	107.1	107.1
	R^2	0.9494	0.9604	0.9641	0.9652	0.9646

HF					
Bond Angle (°)	**X-ray data**	**6-31G(d,p)**	**6-311G(d,p)**	**6-31++G(d,p)**	**6-311++G(d,p)**
N15-C18-N14	124.8	125.1	125.1	124.9	125.0
N13-C16-C19	110.7	109.8	109.8	109.9	109.8
N13-C16-C20	111.0	112.1	112.1	112.1	112.1
C17-C22-F10	112.8	112.7	112.7	112.8	112.8
C17-C21-F9	112.1	112.1	112.2	112.0	112.3
C16-C20-F6	110.9	110.8	110.9	110.8	110.8
C16-C19-F1	112.2	111.7	111.7	111.8	111.8
F10-C22-F11	107.5	108.0	107.9	107.9	108.0
F7-C21-F8	106.1	107.9	107.8	107.8	107.7
F6-C20-F5	107.3	107.8	107.8	107.8	107.7
F1-C19-F2	108.3	107.1	107.1	107.1	107.1
	R^2	0.9604	0.9628	0.9650	0.9641

Table S3. The calculated frequencies (cm^{-1}) and IR intensities of midaflur at B3LYP/6-311++G (d,p) level in gas phase

No	**Assignments (PED%)**	**I_{IR}**	**Unscaled**	**Scaled**
1	$\nu_{as}N_{15}H$ (99)	88.4	3718	3562
2	$\nu N_{13}H$ (100)	56.4	3617	3465
3	$\nu N_{15}H$ (99)	105.6	3595	3444
4	$\nu_{as}N_{14}C_{18}$ (81), sb ($HN_{15}H$) (11)	513.1	1725	1652
5	$\nu N_{14}C_{18}$ (11), asb($H_{24}N_{15}C_{18}$) (11), sb($H_{25}N_{15}H_{24}$) (71)	25.5	1633	1605
6	sb($H_{23}N_{13}C_{17}$) (69)	70.8	1445	1420
7	$\nu_{as}N_{14}C_{18}$ (36), sb($C_{18}N_{14}C_{17}$) (20)	65.7	1422	1398
8	ν ($C_{17}C_{21}$ + $C_{17}C_{22}$) (42)	72.9	1290	1268
9	$\nu C_{16}C_{19}$ (51)	256.7	1262	1240
10	$\nu C_{22}F$ (11), νCC (24)	397.4	1247	1226
11	$\nu C_{19}F$ (19), ν($C_{21}F$+$C_{22}F$) (18)	12.5	1241	1220
12	$\nu C_{16}C_{19}$ (33)	359.1	1236	1215
13	$\nu_{as}C_{20}F$ (40)	208.0	1227	1206
14	$\nu C_{20}F$ (11), ν($C_{21}F$+$C_{22}F$) (26)	222.4	1213	1193
15	ν_{as}($N_{13}C_{16}$ + $N_{14}C_{17}$) (50)	69.3	1191	1171
16	ν_{as} $N_{14}C_{17}$ (42), sb ($H_{24}N_{15}C_{18}$) (20)	391.0	1180	1160
17	$\nu_{as}C_{21}F$ (52), $\nu_{as}N_{13}C_{16}$ (10)	78.1	1158	1139
18	$\nu C_{21}F$ (11), $\nu_{as}N_{13}C_{16}$ (50)	276.9	1153	1134

Table S3. Continues

19	$\nu C_{20}F$ (56)	21.3	1144	1124
20	$\nu_{as}N_{14}C_{17}$ (12), $\nu_{as}C_{19}F_1$ (20)	158.7	1120	1101
21	ν ($C_{21}F$ +$C_{22}F$) (54)	25.9	1118	1099
22	$\nu C_{19}F_1$ (24)	131.0	1110	1092
23	$\nu_{as}(N_{14}C_{18}+N_{15}C_{18})$ (10),$\nu_{as}(N_{13}C_{17}+N_{14}C_{17})$ (15), asb($C_{16}N_{13}C_{17}$) (11)	72.5	1065	1047
24	sb($C_{16}N_{13}C_{17}$) (13), $\nu_{as}N_{14}C_{17}$ (11), $\nu_{as}C_{16}C_{19}$ (17), asb($H_{24}N_{15}C_{18}$) (17)	37.8	1020	1003
25	$\nu C_{16}C$ (25), opb CNCC (15)	194.2	966	950
26	$\nu_{as}CF$ (34), opb CNNC (14)	32.1	958	942
27	$\nu(N_{13}C_{17}+N_{14}C_{17})$ (41), sb($N_{14}C_{17}N_{13}$) (25)	17.6	869	854
28	$\nu_{as}C_{19}F_1$ (10), asb($N_{14}C_{17}N_{13}$) (11)	5.8	760	748
29	$\nu(C_{21}F+C_{22}F)$ (11), $\nu C_{17}N_{13}$ (13)	2.0	745	733
30	$\nu_{as}C_{16}C$ (20),opb NCNC (15)	12.6	731	719
31	sb($C_{18}N_{14}C_{17}$) (14), sb($F_9C_{21}F_8$) (10)	47.6	719	707
32	νCF (16), asb($C_{18}N_{14}C_{17}$) (10), asb($F_{11}C_{22}F_{10}$) (10)	40.5	713	702
33	ν ($N_{13}C_{16}$ + $N_{14}C_{17}$) (18), sb($N_{15}C_{18}N_{14}$) (15), opb CCCC (14)	3.3	663	652
34	opb NCNC (44)	25.9	649	638
35	opb FCFC (12)	0.3	568	559
36	asb($F_9C_{21}F_8$) (21), opb FCFC (19)	0.4	560	551
37	sb($F_{11}C_{22}F_{10}$) (13), opb FCFC (14)	0.3	557	548
38	sb FCF (16)	1.3	554	545
39	sb FCF (12), opb FCFC (10)	0.8	552	543
40	asb FCF (12)	12.1	530	521
41	opb FCFC	1.2	526	518
42	sb($N_{15}C_{18}N_{14}$) (10), sb FCF (25), asb FCF (11)	2.0	509	500
43	χHNCC (62)	4.0	485	477
44	χHNCC (34)	63.0	469	461
45	sb($C_{18}N_{14}C_{17}$) (11)	23.2	437	430
46	opb FCFC	4.8	397	391
47	χHNCC (18), opb CNCC (12)	28.7	382	376
48	νCC (11), asbCCN (10), sbCCN (12), opb CNNC (15)	2.5	374	368
49	sb FCF	0.1	337	331
50	νCC (10)	6.5	322	317
51	asb FCF (12), χHNCC (19), opb FCFC (16)	41.9	310	305
52	χHNCC (20)	50.4	301	296
53	sb FCF (11), asb FCF (11),χHNCC (16), opb FCFC (11), opb FCFC (16)	28.2	292	287
54	sb FCF (14), opb FCFC (11)	8.2	291	286
55	χHNCC (16), opb FCFC (14)	31.2	287	283
56	opb FCFC (12), asb FCFC (12)	10.6	271	267
57	νCC (24), sbCNC (12)	3.6	268	264
58	opb CCCC (35)	1.5	215	212
59	asb CCC (18), sb CCN (14), opb FCFC (11),opb CNCC (11)	1.2	167	165
60	sb $C_{21}CN$ (25), sb $C_{22}CN$ (11), opb FCFC (12)	1.8	159	157
61	sb CCC (47), opb FCFC (12)	2.2	157	155
62	opb CCCC (46)	0.2	153	151
63	opb CNNC (49), opb CNCC (10)	1.8	123	122
64	opb CNNC (13),χCNCN (52)	0.3	88	87
65	χCCCF (89)	0.1	70	69
66	sb CCCC (14), asb CCCC (65)	0.2	65	64
67	asb CCC (13), sb CCN (13), asb CNNC (16), sb CNNC (13)	0.2	58	57
68	χCCCF (90)	0.1	40	40
69	χCCCF (91)	0.1	29	29

ν: symmetric stretching, ν_{as}:asymmetric stretching, χ:torsion, ipb in plane bending, opb:out of plane bending, sb:symmetric bending, asb:asymmetric bending

Table S4. Mulliken atomic charges of Midaflur

	B3LYP/6-311++G(d,p)			B3PW91/6-311++G(d,p)			HF/6-311++G(d,p)		
Atom	Gas	Water	n-Octanol	Gas	Water	n-Octanol	Gas	Water	n-Octanol
F1	-0.05483	-0.05695	-0.05677	-0.00782	-0.00695	-0.00741	-0.10512	-0.10726	-0.10696
F2	-0.02279	-0.04001	-0.03723	-0.00001	-0.01463	-0.01232	-0.09078	-0.10805	-0.10527
F3	-0.04799	-0.06009	-0.05823	-0.01646	-0.03310	-0.03037	-0.11412	-0.12602	-0.12419
F4	-0.02017	-0.02672	-0.02568	0.00605	0.00794	0.00758	-0.07945	-0.08603	-0.08489
F5	-0.04731	-0.05620	-0.05480	0.00424	-0.00738	-0.00549	-0.10639	-0.11527	-0.11385
F6	0.00365	-0.01528	-0.01195	0.00913	0.00190	0.00295	-0.06385	-0.08240	-0.07912
F7	-0.05664	-0.06905	-0.06757	-0.02871	-0.04529	-0.04288	-0.12011	-0.13229	-0.13083
F8	-0.01841	-0.03047	-0.02875	0.00587	-0.00365	-0.00233	-0.08363	-0.09567	-0.09395
F9	-0.04569	-0.06546	-0.06235	-0.01853	-0.03857	-0.03545	-0.10648	-0.12655	-0.12340
F10	-0.03562	-0.05362	-0.05061	-0.00781	-0.02848	-0.02498	-0.09971	-0.11873	-0.11558
F11	0.00291	-0.01343	-0.01070	0.02576	0.01862	0.01963	-0.06317	-0.07896	-0.07632
F12	-0.04515	-0.05460	-0.05340	-0.00195	-0.01313	-0.01159	-0.10051	-0.10993	-0.10872
N13	0.24084	0.23365	0.23125	0.42706	0.35433	0.36772	0.18404	0.18136	0.17866
N14	0.38060	0.28521	0.30212	0.40535	0.28615	0.30695	0.39388	0.28865	0.30710
N15	-0.25627	-0.31305	-0.30467	-0.31763	-0.37072	-0.36301	-0.46099	-0.51281	-0.50508
C16	-0.87062	-0.85169	-0.85531	-1.30078	-1.29456	-1.29558	-0.58424	-0.58099	-0.58252
C17	-4.05797	-3.94429	-3.96336	-4.20902	-4.03579	-4.06686	-4.51082	-4.40054	-4.41991
C18	0.36673	0.36626	0.36758	0.45979	0.46386	0.46404	0.56751	0.58279	0.58177
C19	0.58083	0.59214	0.59118	0.74546	0.75931	0.75775	0.71632	0.73354	0.73146
C20	0.67752	0.69086	0.68807	0.53819	0.56332	0.55839	0.81311	0.83011	0.82680
C21	1.14469	1.14308	1.14365	1.23659	1.21291	1.21743	1.41917	1.41750	1.41825
C22	1.17438	1.17066	1.17086	0.94478	0.94235	0.94259	1.45105	1.45190	1.45171
H23	0.37093	0.42977	0.42126	0.41696	0.49547	0.48146	0.43567	0.49171	0.48356
H24	0.31644	0.36478	0.35729	0.33290	0.37889	0.37132	0.35073	0.39574	0.38883
H25	0.31997	0.37451	0.36812	0.35057	0.40720	0.40045	0.35787	0.40821	0.40244

REFERENCES

[1] Dua, R., Shrivastava, S., Sonwane, S. K., & Srivastava, S. K. (2011). Pharmacological significance of synthetic heterocycles scaffold: a review. *Advances in Biological Research*, 5(3), 120-144.

[2] Purser, S., Moore, P. R., Swallow, S., & Gouverneur, V. (2008). Fluorine in medicinal chemistry. *Chemical Society Reviews*, 37, 320–330.

[3] Tri, N. N., Hailu, Y. M., Duong, L. V., & Nguyen, M. T. (2020). Influence of fluorination on energetic parameters of silole, phosphole, thiophene, oligomers of silole and related acenes.*Journal of Fluorine Chemistry*, 240, 109665.

[4] Bogdanov, A. V., Zaripova, I. F., Voloshina, A. D., Sapunova, A. S., Kulik, N. V., Tsivunina, I. V., Dobrynin, A. B., & Mironov, V. F.(2019). Isatin derivatives bearing a fluorine atom. Part 1: Synthesis, hemotoxicity and antimicrobial activity evaluation of fluoro-benzylated water-soluble pyridinium isatin-3-acylhydrazones. *Journal of Fluorine Chemistry*, 227,109345.

[5] Hong, F., Li, H., Zhu, D., Xia, Z., Zhang, H., Wang, H., & Zeng, Z. (2014). Piperidine and 3,3,4,4,5,5-hexafluoropiperidine as terminal groups: Syntheses and properties as new liquid crystals. *Journal of Fluorine Chemistry*, 168, 61–68.

[6] Lipunova, G. N., Nosova, E. V., Charushin, V. N., & Chupakhin, O. N. (2016). Fluorine-containing indazoles: synthesis and biological activity. *Journal of Fluorine Chemistry*, 192, 1–21.

[7] Uneyama, K., & Sasaki, K. (2009). *Fluorinated heterocyclic compounds: synthesis, chemistry, and applications.* Edited by Viacheslav A. Petrov, John Wiley & Sons, Inc. Publishers, New Jersey.

[8] Uneyama, K. (2006). *Fluorine in drug designs. Organofluorine Chemistry*; Blackwell Publishing: Oxford, UK.
[9] Inoue, M., Sumii, Y., & Shibata, N. (2020). Contribution of organofluorine compounds to pharmaceuticals. *ACS Omega*, 5, 10633−10640.
[10] Middleton, W. J., & Krespan, C. G. (1970). Fluorinated aminoimidazolines.Synthesis and determination of tautomeric structure. *Journal of Organic Chemistry*, 35, 1480-1485.
[11] Guggenberger, L. J. (1973). The crystal structure of 4-amino-2,2,5,5-tetrakis(trifluoromethyl)-3-imidazoline. *Acta Crystallographica Section B*, B29, 2110-2114.
[12] Arora, S. K.(1981). Structure of a complex of midaflur (a central nervous system depressant) and dimethyl sulfoxide. *Acta Crystallographica Section B*, B37, 2052-2055.
[13] Levine, I. M., Jossmann, P. B.., Friend, D. G., & DeAngelis, V. (1968). Effect of 5-imino-2,2,4,4-tetrakis (trifluoromethyl) imidazolidine (EXP 338) on spasticity: A quantitative evaluation.*Clinical Pharmacology & Therapeutics*, 9(4), 448-455.
[14] Clark, R., Lynes, T. E., Price, W. A., Smith, D. H., Woodward, J. K., Marvel, J. P., V.G. & Vernier, V. G. (1971). The pharmacology and toxicology of midaflur.*Toxicology and Applied Pharmacology*, 18, 917-943.
[15] Borges, R. M., Colby, S. M., Das, S., Edison, A. S., Fiehn, O., Kind, T., Lee, J., Merrill, A. T., Merz, K. M. Jr., Metz, T. O., Nunez, J. R., Tantillo, D. J., Wang, L. P., Wang, S., & Renslow, R. S. (2021). Quantum chemistry calculations for metabolomics. *Chemical Reviews*, 121(10), 5633–5670.
[16] Feizi-Dehnayebi, M., Dehghanian, E., & Mansouri-Torshizi, H. (2021). DNA/BSA binding affinity studies of new Pd (II) complex with S-S and N-N donor mixed ligands via experimental insight and molecular simulation: Preliminary antitumor activity, lipophilicity and DFT perspective. *Journal of Molecular Liquids*, 344(1), 117853.
[17] Serdaroğlu, G., & Elik, M. (2018). A computational study predicting the chemical reactivity behavior of 1-substituted 9-ethyl-βCCM derivatives: DFT- based quantum chemical descriptors.*Turkish Computational and Theoretical Chemistry*, 2(1), 1-11.
[18] Sayın, K., & Üngördü, A., (2019). Investigations of structural, spectral and electronic properties of enrofloxacin and boron complexes via quantum chemical calculation and molecular docking. *Spectrochimica Acta Part A: Molecular and Biomolecular Spectroscopy*, 220, 117102.
[19] Serdaroğlu, G., & Ortiz, J. V. (2017). Ab initio calculations on some antiepileptic drugs such as phenytoin, phenobarbital, ethosuximide and carbamazepine.*Structural Chemistry*, 28, 957-964.
[20] Üngördü, A., & Sayın, K. (2019). Quantum chemical calculations on sparfloxacin and boron complexes. *Chemical Physics Letters*, 733, 136677.
[21] Feizi-Dehnayebi, M., Dehghanian, E., & Mansouri-Torshizi, H. (2021). Synthesis and characterization of Pd (II) antitumor complex, DFT calculation and DNA/BSA binding insight through the combined experimental and theoretical aspects.*Journal of Molecular Structure*, 1240, 130535.
[22] Frisch, M. J., Trucks, G. W., Schlegel, H. B., Scuseria, G. E., Robb, M. A., Cheeseman, J. R., Scalmani, G., Barone, V., Petersson, G. A., Nakatsuji, H., Li, X., Caricato, M., Marenich, A. V., Bloino, J., Janesko, B. G., Gomperts, R., Mennucci, B., Hratchian, H. P., Ortiz, J.V., Izmaylov, A. F., Sonnenberg, J. L., Williams-Young, D., Ding, F., Lipparini, F., Egidi, F., Goings, J., Peng, B., Petrone, A., Henderson, T., Ranasinghe, D., Zakrzewski, V. G., Gao, J., Rega, N., Zheng, G., Liang, W., Hada, M., Ehara, M., Toyota, K., Fukuda, R., Hasegawa, J., Ishida, M., Nakajima, T., Honda, Y., Kitao, O., Nakai, H., Vreven, T., Throssell, K., Montgomery, J. A. Jr., Peralta, J. E., Ogliaro, F., Bearpark, M. J., Heyd, J. J., Brothers, E. N., Kudin, K. N., Staroverov, V. N., Keith, T. A., Kobayashi, R., Normand, J., Raghavachari, K., Rendell, A. P., Burant, J. C., Iyengar, S. S., Tomasi, J., Cossi, M., Millam, J. M., Klene, M., Adamo, C., Cammi, R., Ochterski, J. W., Martin, R. L.,Morokuma, K., Farkas, O., Foresman, J. B., Fox, D. J., Gaussian 09, Rev.D.01, Gaussian, Inc., Wallingford CT, 2009.
[23] Becke, A. D. (1993). A new mixing of Hartree–Fock and local density functional theories.*Journal of Chemical Physics*, 98, 1372–1377.
[24] Lee, C., Yang, W., & Parr, R. G. (1988). Development of the Colle-Salvetti correlation-energy formula into a functional of the electron density.*Physical Review B*, 37, 785–789.
[25] Becke, A. D. (1993). Density- functional thermochemistry. III. The role of exact exchange.*Journal of Chemical Physics*, 98: 5648–5652.
[26] Perdew, J. P., Chevary, J. A., Vosko, S. H., Jackson, K. A., Pederson, M. R., Singh, D. J., & Fiolhais, C. (1992). Atoms, molecules, solids, and surfaces: Applications of the generalized gradient approximation for exchange and correlation. *Physical Review B*, 46, 6671-6687.

[27] Roothaan, C. C. J. (1951). New Developments in Molecular Orbital Theory. *Reviews of Modern Physics*, 23, 69-89.
[28] Jamroz, M. H. Vibrational Energy Distribution Analysis VEDA 4, Warsaw, 2004–2010.
[29] Dennington, R., Keith, T., Millam, J., Gauss View, Version 5., Semichem Inc., Shawnee Mission, KS. 2009.
[30] O'Boyle, N. M., Tenderholt, A. L., Langer, K. M. (2008). Cclib: A library for package-independent computational chemistry algorithms. *Journal of Computational Chemistry*, 29, 839-845.
[31] Marenich, A. V., Cramer, C. J., & Truhlar, D. G. (2009). Universal solvation model based on solute electron density and on a continuum model of the solvent defined by the bulk dielectric constant and atomic surface tensions. *Journal of Physical Chemistry B*, 113(18), 6378-6396.
[32] Janeoo, S., Reenu, Saroa, A., Kumar, R., & Kaur, H. (2022). Computational investigation of bioactive 2,3-diaryl quinolines using DFT method: FT- IR, NMR spectra, NBO, NLO, HOMO-LUMO transitions, and quantum-chemical properties. *Journal of Molecular Structure*, 1253, 132285.
[33] Sundaraganesan, N., Ilakiamani, S., Salem, H., Wojciechowski, P. M., & Michalska, D. (2005). FT-Raman and FT-IR spectra, vibrational assignments and density functional studies of 5-bromo-2-nitropyridine. *Spectrochimica Acta Part A: Molecular and Biomolecular Spectroscopy*, 61, 2995–3001.
[34] Mulliken, R. S. (1955). Electronic Population Analysis on LCAO-MO Molecular Wave Functions. I. *Journal of Chemical Physics*, 23, 1833-1840.
[35] Fukui, K. (1982). The Role of frontier orbitals in chemical reactions.*Science*, 218, 747–754.
[36] Fradi, T., Noureddine, O., Taheur, F. B., Guergueb, M., Nasri, S., Amiri, N., Almahri, A., Roisnel, T., Guerineau, V., Issoui, N., & Nasri, H. (2021). New DMAP meso-arylporphyrin Magnesium (II) complex.spectroscopic, cyclic voltammetry and X-ray molecular structure characterization. DFT, DOS and MEP calculations and Antioxidant and Antifungal activities. *Journal of Molecular Structure*, 1236, 130299.
[37] Eşme, A. (2017). Theoretical studies of molecular structure, spectroscopic, electronic and NLO investigations of Oxamyl. *Journal of Balıkesir University Institute of Science and Technology*, 19(2), 99-115.
[38] Koopmans, T. (1934). Über die zuordnung von wellenfunktionen und eigenwertenzu den einzelnen elektronen eines atoms. *Physica*, 1, 104-113.
[39] Parr, R. G., & Pearson, R. G. (1983). Absolute hardness: companion parameter to absolute electronegativity. *Journal of the American Chemical Society*, 105, 7512-7516.
[40] Pearson, R. G. (1986). Absolute electronegativity and hardness correlated with the molecular orbital theory. *Proceedings of the National Academy of Sciences of the USA*, 83, 8440-8441.
[41] Parr, R. G., Szentpaly, L. V., & Liu, S. (1999). Electrophilicity Index. *Journal of the American Chemical Society*, 121, 1922-1924.
[42] Perdew, J. P., & Levy, M. (1983). Physical content of the exact Kohn-Sham orbital energies: band gaps and derivative iscontinuities. *Physical Review Letters*, 51(20), 1884-1887.
[43] Perdew, J. P., Parr, R. G., Levy, M., & Balduz, J. L. Jr. (1982). Density functional theory for fractional particle number: derivative discontinuities of the energy. *Physical Review Letters*, 49(23), 1691-1694.
[44] Clark, T., Chandrasekhar, J., Spitznagel, G. W., & Schleyer, P. V. R. (1983). Efficient diffuse function-augmented basis sets for anion calculations. III.* The 3-21+G basis set for first-row elements, Li-F. *Journal of Computational Chemistry*, 4, 294-301.
[45] Guthrie, J. P. (2009). A blind challenge for computational solvation free energies: introduction and overview. *Journal of Physical Chemistry B*, 113, 4501–4507.
[46] Klimovich, P. V., & Mobley, D. L. (2010). Predicting hydration free energies using all-atom molecular dynamics simulations and multiple starting conformations. *Journal of Computer-Aided Molecular Design*, 24, 307–316.
[47] Matos, G. D. R., Kyu, D. Y., Loeffler, H. H., Chodera, J. D., Shirts, M. R., & Mobley, D. L. (2017). Approaches for calculating solvation free energies and enthalpies demonstrated with an update of the FreeSolv database. *Journal of Chemical & Engineering Data*, 62(5), 1559–1569.
[48] Michalík, M., & Lukeš, V. (2016). The validation of quantum chemical lipophilicity prediction of alcohols. *Acta Chimica Slovaca*, 9(2), 89-94.
[49] Elik, M., & Serdaroğlu, G. (2017). A computational study of 1-substituted methyl 9-methyl-9H-pyrido[3,4-b]indole-3-carboxylate: quantum chemical descriptors, FMO and NBO analysis. *Cumhuriyet Science Journal*, 38(4), 138-155.
[50] Serdaroğlu, G., & Elik, M. (2017). DFT based quantum chemical descriptors of 1-substituted THβC, DHβC, βC derivatives. *Cumhuriyet Science Journal*, 38(4), 647-660.
[51] Van De Waterbeemd, H., & Gifford, E. (2003). ADMET in silico modelling:towards prediction paradise?. *Nature Reviews Drug Discovery*, 2(3), 192-204.

[52] Van de Waterbeemd, H., Smith, D. A., & Jones, B. C. (2001).Lipophilicity in PK design: methyl, ethyl, futile.*Journal of Computer-Aided Molecular Design*, 15, 273-286.
[53] Foresman, J. B., & Frisch, Æ. (2015). *Exploring chemistry with electronic structure methods*, third edition, Gaussian, Inc. Wallingford, CT USA.
[54] Bohnert, T., & Prakash, C. (2012). ADME profiling in drug discovery and development: an overview. *Encyclopedia of Drug Metabolism and Interactions*, 1-35.
[55] Garrido, N. M., Queimada, A. J., Jorge, M., Macedo, E. A., Ioannis, G., & Economou, I. G. (2009). 1-Octanol/water partition coefficients of n-alkanes from molecular simulations of absolute solvation free energies. *Journal of Chemical Theory and Computation*, 5, 2436-2446.
[56] Hansch, C., Björkroth, J. P., & Leo, A. (1987). Hydrophobicity and central nervous system agents: on the principle of minimal hydrophobicity in drug design. *Journal of Pharmaceutical Sciences*, 76(9), 663-687.
[57] Weinhold, F., Landis, C. R., & Glendening, E. D. (2016). What is NBO analysis and how is it useful?. *International Reviews in Physical Chemistry*, 35(3), 399-440.
[58] Reed, A. E., Curtiss, L. A., & Weinhold, F. (1988). Intermolecular interactions from a natural bond orbital, donor-acceptor viewpoint. *Chemical Reviews*, 88(6), 899-926.
[59] Hurst, M., & Munn, R. W. (1989).*In Organic Materials for Nonlinear Optics;* R.A. Hann, D. Bloor, Eds.; The Royal Society of Chemistry: London.
[60] Garza, A. J., Osman, O. I., Asiri, A. M., & Scuseria, G. E. (2015). Can gap tuning schemes of long-range corrected hybrid functionals improve the description of hyperpolarizabilities?. *Journal of Physical Chemistry B*, 119, 1202−1212.
[61] Rajeshirke, M., & Sekar, N. (2018). NLO properties of ester containing fluorescent carbazole based styryl dyes-consolidated spectroscopic and DFT approach. *Optical Materials*, 76, 191-209.
[62] Abraham, J. P., Sajan, D., Hubert, I. J., & Jayakumar, V. S. (2008). Molecular structure, spectroscopic studies and first-order molecular hyperpolarizabilities of p-amino acetanilide. *Spectrochimica Acta, Part A: Molecular and Biomolecular Spectroscopy*, 71, 355-367.
[63] Karamanis, P., Pouchan, C., & Maroulis, G. (2008). Structure, stability, dipole polarizability and differential polarizability in small gallium arsenide clusters from all-electron ab initio and density-functional-theory calculations. *Physical Review A*, 77, 013201-013203.
[64] Ahmed, A. B., Feki, H., Abid, Y., Boughzala, H., & Mlayah, A. (2008). Structural, vibrational and theoretical studies of l-histidine bromide. *Journal of Molecular Structure*, 888(1-3), 180-186.
[65] Sethi, A., & Prakash, R. (2015). Novel synthetic ester of Brassicasterol, DFT investigation including NBO, NLO response, reactivity descriptor and its intramolecular interactions analyzed by AIM theory. *Journal of Molecular Structure*, 1083, 72-81.
[66] Shahid, M., Salim, M., Khalid, M., Tahir, M. N., Khan, M. U., & Braga, A. A. C. (2018). Synthetic, XRD, non-covalent interactions and solvent dependent nonlinear optical studies of sulfadiazine-ortho-vanillin schiff base: (E)-4-((2-hydroxy-3-methoxy- benzylidene) amino)-*N*-(pyrimidin-2-yl) benzene-sulfonamide. *Journal of Molecular Structure*, 1161, 66-75.
[67] Murray, J. S., & Politzer, P. (2011). The electrostatic potential: an overview. *Wiley Interdisciplinary Reviews: Computational Molecular Science*, 1, 153-322.
[68] Murray, J., & Sen, K. (1996). *Molecular electrostatic potentials: concepts and applications*, 1 st edition, Elsevier, Amsterdam.
[69] Scrocco, E., & Tomasi, J. (1978). Electronic molecular structure, reactivity and intermolecular forces: a euristic interpretation by means of electrostatic molecular potentials. *Advances in Quantum Chemistry*, 11, 115-193.